AD-F300 466

⑫

AD

TECHNICAL REPORT ARBRL-TR-02573

INSTRUMENTATION TECHNIQUES FOR MEASURING
LARGE, HIGH RATE STRAINS WITH FOIL
RESISTANCE STRAIN GAGES

AD-A146 248

Edward J. Rapacki, Jr.

August 1984

US ARMY ARMAMENT RESEARCH AND DEVELOPMENT CENTER
BALLISTIC RESEARCH LABORATORY
ABERDEEN PROVING GROUND, MARYLAND

DTIC FILE COPY

OCT 1 5 1984

E

REPORT DOCUMENTATION PAGE		READ INSTRUCTIONS BEFORE COMPLETING FORM
1. REPORT NUMBER Technical Report ARBRL-TR-02573	2. GOVT ACCESSION NO. AD/1146.34{	3. RECIPIENT'S CATALOG NUMBER
4. TITLE (and Subtitle) INSTRUMENTATION TECHNIQUES FOR MEASURING LARGE, HIGH RATE STRAINS WITH FOIL RESISTANCE STRAIN GAGES		5. TYPE OF REPORT & PERIOD COVERED FINAL
		6. PERFORMING ORG. REPORT NUMBER
7. AUTHOR(s) Edward J. Rapacki, Jr.		8. CONTRACT OR GRANT NUMBER(s)
9. PERFORMING ORGANIZATION NAME AND ADDRESS US Army Ballistic Research Laboratory ATTN: DRXBR-TBD Aberdeen Proving Ground, MD 21005-5066		10. PROGRAM ELEMENT. PROJECT, TASK AREA & WORK UNIT NUMBERS 1L161102AH43
11. CONTROLLING OFFICE NAME AND ADDRESS US Army Ballistic Research Laboratory ATTN: DRXBR-OD-ST Aberdeen Proving Ground, MD 21005-5066		12. REPORT DATE August 1984
		13. NUMBER OF PAGES 53
14. MONITORING AGENCY NAME & ADDRESS(if different from Controlling Office)		15. SECURITY CLASS. (of this report) UNCLASSIFIED
		15a. DECLASSIFICATION/DOWNGRADING SCHEDULE

16. DISTRIBUTION STATEMENT (of this Report)

   Approved for public release; distribution unlimited.

17. DISTRIBUTION STATEMENT (of the abstract entered in Block 20, if different from Report)

18. SUPPLEMENTARY NOTES

19. KEY WORDS (Continue on reverse side if necessary and identify by block number)

Instrumentation
Pulse Excitation
Wheatstone Bridge
Strain Gages
High Strain-rate Response

Strain Gage Power Density
Impact Test Facility Instrumentation

20. ABSTRACT (Continue on reverse side if necessary and identify by block number)
Instrumentation for measuring large, high strain rate strains with foil type resistance strain gages was designed, constructed and evaluated in terms of signal to noise ratio, strain rate response characteristics and overall accuracy of measurement. Complete design procedures and component specifications for the Wheatstone bridge, pulsed power supply and control circuit, as well as calibration and data reduction procedures are included. The apparatus has a signal to noise ratio up to six times that which can be obtained with conventional strain gage signal conditioning equipment, and can measure to $\pm$ 0.20 strain at strain

DD FORM 1473 EDITION OF 1 NOV 65 IS OBSOLETE

rates up to 10^4 s^{-1} over a 35 to 200 microsecond sample time. The overall accuracy of measurement is $\pm$ (1.4 percent ϵ + 375 microstrain), with 110 microstrain resolution. Pulsed power density limits for annealed constantan foil strain gages were also investigated and are reported.

TABLE OF CONTENTS

Page

Accession For

3

LIST OF ILLUSTRATIONS

I. INTRODUCTION

Resistive element transducers, such as strain gages, manganin pressure gages and nickel temperature sensors are used extensively in experimental stress analysis. The variable of interest (deformation, pressure, or temperature change) causes a change of sensor resistance, which must be measured. Using the sensor as an arm of a Wheatstone bridge network is the most sensitive circuit for measuring these often small resistance changes. Often too, these measurements must be made in environments where electrical "noise" may be severe enough to distort or obscure the signal of interest, even after proper grounding and shielding techniques have been employed.[1] Greater signal strength is required also when digital signal acquisition techniques are used because of the inherent loss of voltage sensitivity and resolution. The ease of data acquisition and reduction, however, make digital techniques very desirable, particularly for multiple channels of single, transient events. Signal strength, and hence signal to noise ratio (S/N), can be improved by increasing the excitation voltage of the bridge; however, power dissipation capability of the sensor and allowable thermally induced drift place constraints on the maximum allowable continuous excitation voltage.[2]

Pulse excitation of the sensor allows higher excitation voltage without the attendant difficulties of continuous high power dissipation. The technique can be used where a relatively short duration (up to a few hundred microseconds) measurement is required or where a series of short sample time, intermittent measurements is satisfactory.

This report describes the design of a Wheatstone bridge, power supply and associated control circuitry for use with pulse excited resistive element transducers. The specific application was the measurement of high rate, post yield strains with foil resistance strain gages on long rods undergoing high velocity impact. Performance tests, calibration and data reduction procedures and an overall error analysis are included.

II. DESIGN CONSIDERATIONS

A. Strain Gages

Foil resistance strain gages are available in a multitude of alloys, gage lengths and geometries. The measurement of very high rate ($>10^4$ s^{-1}), post-yield strains up to 20 percent, however, requires short gage length and a very ductile alloy. Micro-Measurements type EP gages, which are an annealed

---

[1] Ralph Morrison, *Grounding and Shielding Techniques in Instrumentation*, 2nd ed., John Wiley and Sons, Inc., New York, Chichester, Brisbane, Toronto, 1977.

[2] Measurements Group, Inc., *Optimizing Strain Gage Excitation Levels*, Technical Note No. TN-502, Raleigh, NC, 1979.

constantan foil on a polyimide backing were chosen. Sharpe[3] shows that 1.57 mm gage length foil gages have response characteristics comparable to dynamic optical strain gages, whose gage lengths are as short as 0.127 mm and Hauver and Melani[4] report that they can respond to compressive strains in excess of 20 percent. Initial, unstrained resistance was 120.0 ohms to simultaneously maximize bridge sensitivity and facilitate proper termination of the gage to bridge connecting cable. Both single element and planar rosette gage patterns are usable; stacked rosettes are not recommended for high power excitation due to their decreased power dissipation capability.[2]

B. Wheatstone Bridge

The Wheatstone bridge network, Figure 1, consists of one active arm R_1, which includes the gage resistance R_g, and connecting cable and gage lead resistance R_x. The remaining arms (R_2, R_3, and R_4) provide a network to balance the bridge for an initial null output and provide proper termination for the connecting cable used. R_5 is the input impedance of the output voltage measuring device, an oscilloscope. E_{in} is a constant DC excitation voltage from a low impedance source. By necessity, pulsed excitation requires the bridge be used in the unbalanced condition, the theory of which, for example, is shown by Perry and Lissner.[5] Referring to Figure 1, bridge output voltage is given by

$$E_{out} = E_{in} \left(\frac{R_1}{R_1 + R_4} - \frac{R_2}{R_2 + R_3} \right)$$

(1)

if R_5 is an infinite impedance. For finite values of R_5, the output voltage is attenuated, and the measured output is

$$E_{meas} = \frac{R_5}{Z} E_{out}$$

(2)

[3] W. N. Sharpe, Jr., "Dynamic Plastic Response of Foil Gages," Experimental Mechanics, Vol. 10, No. 10, October 1970, pp. 408-414.

[4] G. E. Hauver and A. Melani, "Strain-Gage Techniques for Studies of Projectile Behavior During Penetration," Ballistic Research Laboratory Memorandum Report No. ARBRL-MR-03082, February 1981. ADA 098660

[5] C. C. Perry and H. R. Lissner, The Strain Gage Primer, McGraw-Hill Book Co., Inc., New York, Toronto, London, 1955, pp. 48-51.
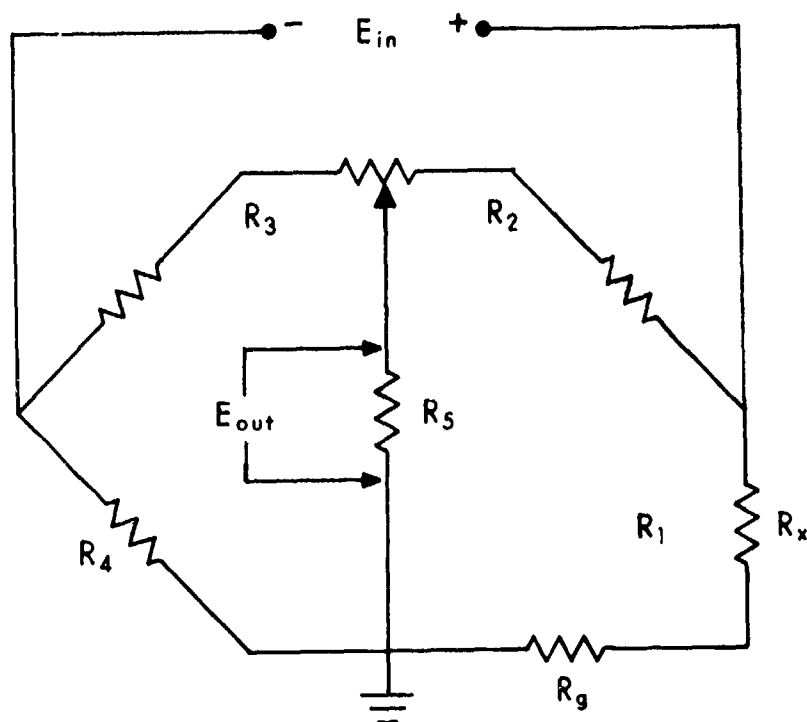
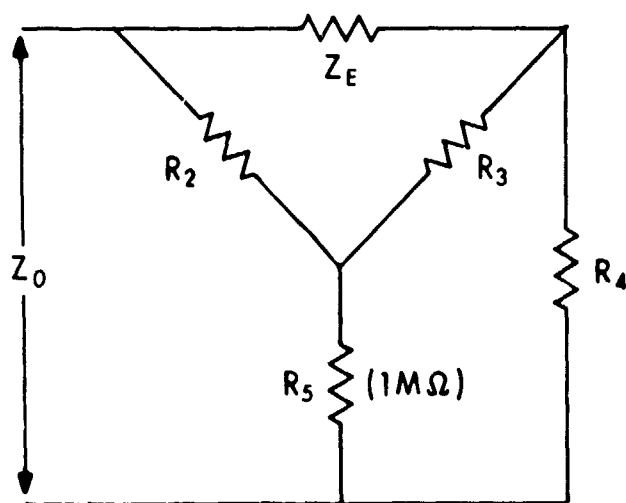Figure 1. Mathematical Schematic of Wheatstone Bridge Network.

Figure 2. Mathematical Schematic of Gage to Bridge Coaxial Cable
Termination.

where

$$Z = R_5 + \frac{(R_1 + R_2) \cdot (R_3 + R_4)}{R_1 + R_2 + R_3 + R_4}$$

(3)

by the rules for parallel conductors. If the second term of Eq. 3 is much, much smaller than R_5, $Z \simeq R_5$ and $E_{meas} = E_{out}$ to a very close approximation. Note that if a coaxial cable is used to connect bridge output to the oscilloscope, R_5 should be the cable's characteristic impedance. This makes both terms of Eq. 3 of the same order of magnitude, and considerable (and for large variations of R_1, non-linear) attenuation of E_{out} occurs. Thus, direct connection of bridge output to a high impedance (one megohm) input, sans cable, is preferred.

Depending on the type of high strain rate experiment being performed, the gage to bridge connecting cable may need to be quite long. Cable selection is done at this stage of the design because the bridge completion resistors and power supply form the cable termination, which should be the characteristic impedance. Figure 2 shows what the gage cable "sees" as impedance Z_o at the bridge end. If the impedance of the voltage source, Z_E is assumed negligible, $Z_o \simeq R_4$ for values of R_4 much less than one megohm.

Differentiating Eq. 1 with respect to gage arm resistance R_1 yields an expression for bridge sensitivity, which should be maximized. It can be shown that this is achieved when $R_4 = R_1$, approximately 120 ohms. Thus, cable characteristic impedance should be close to this value. Also, low attenuation (air-spaced) cables are preferred. Thus, the choice is limited to RG-63/U (125 ohm) and RG-62/U (93 ohm) coaxial cable. The latter was chosen because of its ease of handling (smaller diameter), ready availability, and decreased cost. Signal transmission characteristics of both cables are comparable, while bridge sensitivity is decreased only 1.5 percent using 93 rather than 125 ohms for R_4.

Before power dissipation specifications for the bridge completion resistors can be determined, maximum excitation voltage must be established. The primary consideration is gage stability. Reference 2 provides guidance in this matter, but an experimental determination of maximum excitation voltage under which tolerable gage resistance instability occurs should be performed. The resistance instability manifests itself as "apparent strain," that is, a purely temperature induced change of gage resistance. Pulsed excitation for short periods causes non-equilibrium heating of the gage grid material, backing, glue line and substrate specimen material. Apparent strain vs temperature curves supplied by gage manufacturers cannot be used as correction factors because their tests are performed at equilibrium temperatures. Appendix A details power dissipation limits for pulse excited annealed

10

constantan foil strain gages mounted on steel. A power density (P_D) of 0.235 W/mm^2 causes bridge output to drift approximately 0.3 microstrain per microsecond of excitation. The active area of the grid (A_g, gage length X grid width, mm^2) is used in the calculation, and acceptable excitation voltage is given by Eq. 4.

$$E_{in} = \sqrt{\frac{P_D \times A_g}{R_g}} \; (R_g + R_x + R_4) \tag{4}$$

The use of strain gages with gage lengths longer than 3.18 mm and grid widths in excess of 4.57 mm would be inconsistant with the dynamic measurement requirements, thus the remaining bridge and power supply components are designed for a maximum operating voltage of 36 volts, while 15 volts is used for the 1.57 mm square gages. Continuous excitation would limit the voltage to about 5.5 for this size gage, thus S/N is improved by a factor of better than 2.7.

Equation 1 shows that bridge output can vary because of resistance changes in R_g, the intended measurement, and changes in any of the bridge completion resistors. For this reason, high stability, low noise resistors with fast risetime characteristics are desired. Deposited metal film resistors meet these requirements, and have the power dissipation capability needed. For example, R_4, which is 93 ohms, requires a short term power rating in excess of 14 watts; this situation arises should the gage become shorted. A ten watt, 50 percent overload for five seconds maximum, metal film resistor is available in a heat sinkable standard TO-3 package at modest cost. The upper bridge arm resistors, R_2 and R_3, are chosen to make the second term in Eq. 3 much, much smaller than one megohm, yet large enough to keep current drain on the power supply small. Additionally, portions of these two resistances must be embodied in a tapped potentiometer to initially balance the bridge. A ten turn, wirewound potentiometer provides good balance resolution if the variable portions of R_2 and R_3 are about ten percent of their total values. Values of 690 and 515 ohms were used for the fixed portions of R_2 and R_3, respectively, using one watt metal film resistors. The balancing potentiometer is 100 ohms, two watt, with eight microhenry inductance. By Eqs. 1 thru 3, bridge output voltage is attenuated less than 3.5×10^{-3} dB. Nominal impedance of the bridge is 185 ohms when balanced for a 120 ohm gage. The balancing sensitivity is such that a 120 ohm gage can be balanced to ± 0.010 ohms, or ± 45 microstrain. Figure 3 is a graph of normalized bridge output vs change of gage resistance and can be used to estimate expected signal levels for given resistance changes and excitation voltages.
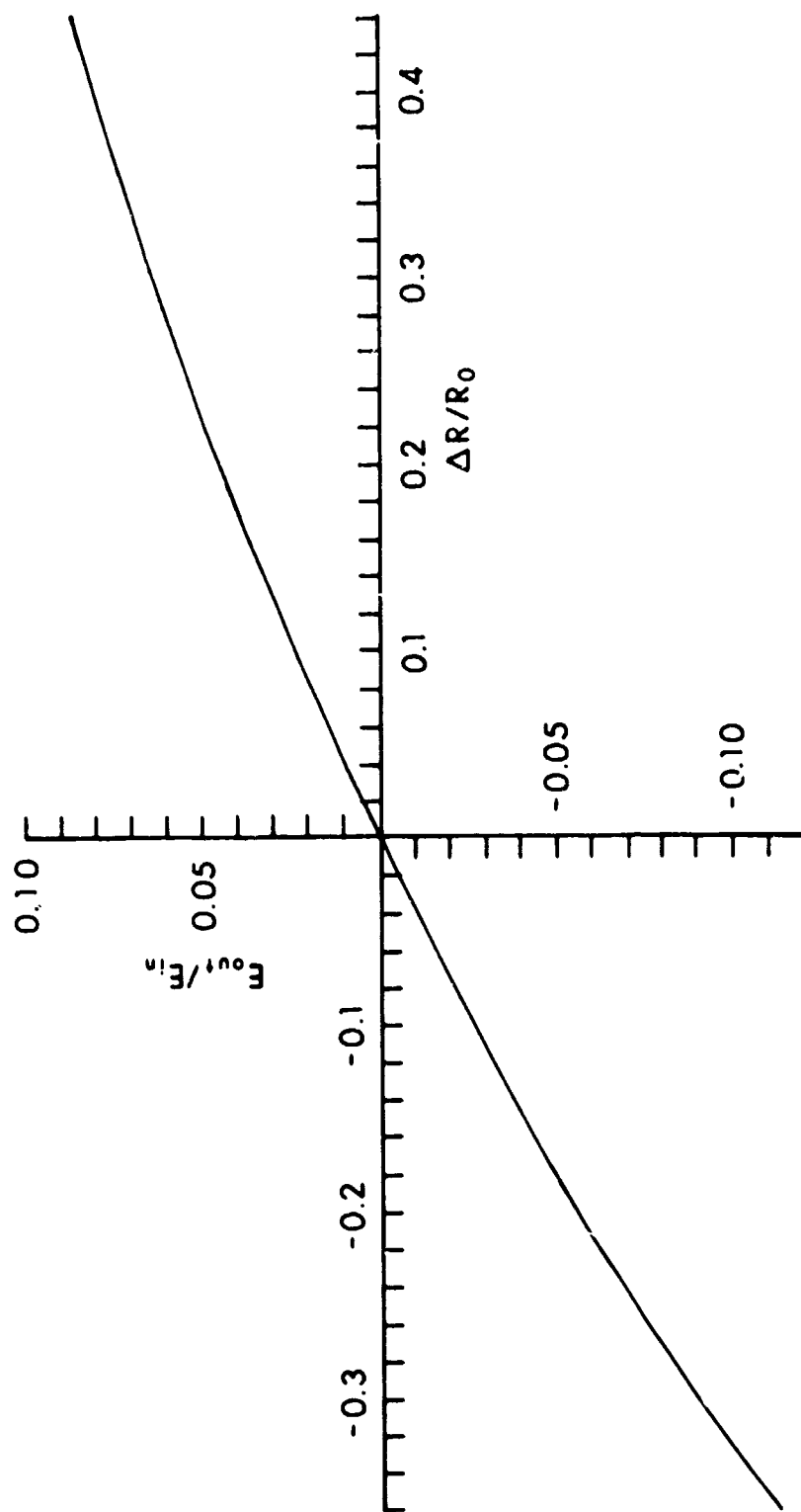
11

Figure 5. Normalized Bridge Output Voltage vs Change in Resistance of 120.0 Ohm Gage.

C. Pulse Power Supply

The pulse power supply is of the voltage regulated, capacitive discharge type. See Figure 4 for schematic diagram. The voltage to which the capacitor is initially charged (the desired excitation voltage) is regulated by a five percent tolerance zener diode. Capacitor size requirements depend upon the degree of discharge voltage stability required and pulse duration. Stability requirements are directly related to the bridge output voltage resolution, which must be on the order of the balance resolution. For the bridge designed, the minimum output resolution should be ± 0.8mV. This is the minimum resolvable with an 8-bit digital oscilloscope on the ± 100 mV scale, and is ± 0.4 percent of full scale. Bridge output voltage for constant load should be constant to this percentage extent, as should excitation voltage due to the direct proportionality. Pulse duration requirements greater than 200 microseconds were not anticipated, so a 470 microfarad electrolytic capacitor, discharging into a nominal bridge load of 185 ohms, provides the required voltage stability over this time. Batteries are used to charge the capacitor since the power supply must float with respect to ground when single-ended amplifiers are used. This also eliminates cross-talk problems associated with a common charging supply when multiple channels are used. Charging resistors (15 K-ohm) are chosen to minimize battery drain while supplying sufficient current so the zener diode regulates properly, and initial charge up time is reasonable, about 60 seconds.

An NPN Si power transistor (2N3441)[6] is used as the switch to turn the bridge excitation voltage on and off. Current flows from the capacitor thru the transistor as collector current, I_C, to the bridge load. Sufficient base current, I_B, must be provided so the power transistor is conducting in its low forward impedance range over the expected range of I_C. The base current is provided by a nine volt battery thru the phototransistor of an optocoupler (TIL117)[7] in a modified Darlington configuration. The resistance-capacitance network in the base current circuit limits the rate of I_B, and provides a "soft start" for the power supply. This soft start is required because high current slewing rates, even thru small reactances* in the bridge circuit, produce back emf overshoots at the bridge output. These overshoots can saturate sensitive oscilloscope preamplifiers to the point where instability and drift seriously affects the measurement. The soft start does increase the turn-on response time, (see Performance Tests, below) but this can be dealt with by trigger control circuitry, described below.

---

[6]*Radio Corporation of America, Inc., Power Transistors, Databook No. SSD-204C, Somerville, NJ, 1974, pp. 103-115.*

[7]*Texas Instruments, Inc., The Optoelectronics Data Book for Design Engineers, 5th ed., Dallas, TX, 1978, pp. 114-118.*

The RG-62/U coaxial cable presents the largest unbalanced inductance in the bridge circuit, $0.41\,\mu H/m$. Thus, even modest cable lengths can add significant reactance.
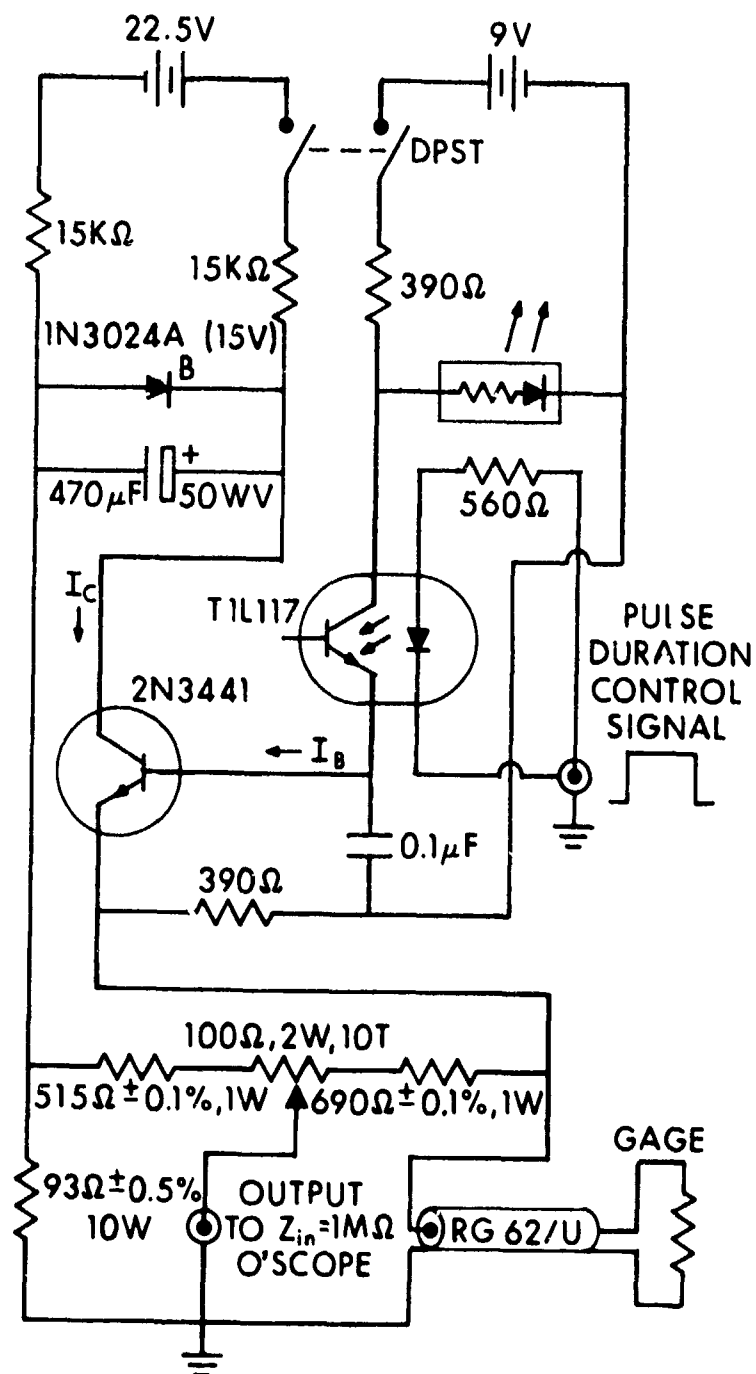
Figure 4. Schematic Diagram of Pulse Power Supply and Wheatstone
Bridge Circuit.

The optocoupler provides the necessary isolation between the floating base current circuit and the common pulse duration control signal. The control signal is the forward current thru the photodiode of the optocoupler and is a timed DC pulse.

D. Control Circuit

The control circuit schematic for the pulse power supply and oscilloscope trigger is shown in Figure 5. It is a sequential timer using MC1455P1 integrated timing circuits,[8] and the input trigger requirement is compatible with TTL levels. (A time-domain pre-event trigger circuit that is useful for triggering instrumentation in impact tests is described in Appendix B.) A negative edge trigger at the 47 picofarad input coupling capacitor triggers timer IC1 and 2. IC1 sources current to the 2N3441 power transistor base, and the collector current is the control signal. The power transistor is used because it was desired to control up to 14 pulse power supplies simultaneously, requiring more current than the timer IC itself could source. The duration of the control signal is variable from 5 to 450 microseconds and is controlled by the 25K-ohm potentiometer. IC2 provides a delay of 10 to 300 microseconds before IC3 is triggered, which provides a > +10vdc signal to trigger the oscilloscopes and/or other instrumentation. This delay between power supply turn-on and oscilloscope trigger allows the power supply and bridge circuit to stabilize before recording any of the output signal, thus conserving record length and providing a common timing reference point.

III. PERFORMANCE TESTS

The performance tests on the power supply, switching circuit and bridge were performed using a five watt, one percent tolerance, 120 ohm metal film resistor as a substitute for the strain gage. This allowed a broad range of tests to be performed without concern for limitations imposed by the strain gage itself. Except where noted, all tests were performed in situ, that is, pulsed on with the control circuit and the Wheatstone bridge was the load. The gage substitute was connected to the bridge with 14 meters of RG-62/U coaxial cable, which added 2.55 ohms series resistance to the gage arm. The desired range of strain measurement is $\pm$ 20 percent, the upper limit of epoxy-based strain gage adhesives. Strain ϵ, is calculated using

$$\epsilon = \sqrt{R_g/R_o} - 1$$

(5)

where R_g is the resistance of the strained gage, and R_o is the initial, unstrained resistance. This expression for strain results when $(2 + \epsilon)$ is

[8]Motorola, Inc., *Linear Integrated Circuits*, Series C, Phoenix, AZ, 1979, pp. 6-44 - 6-50.
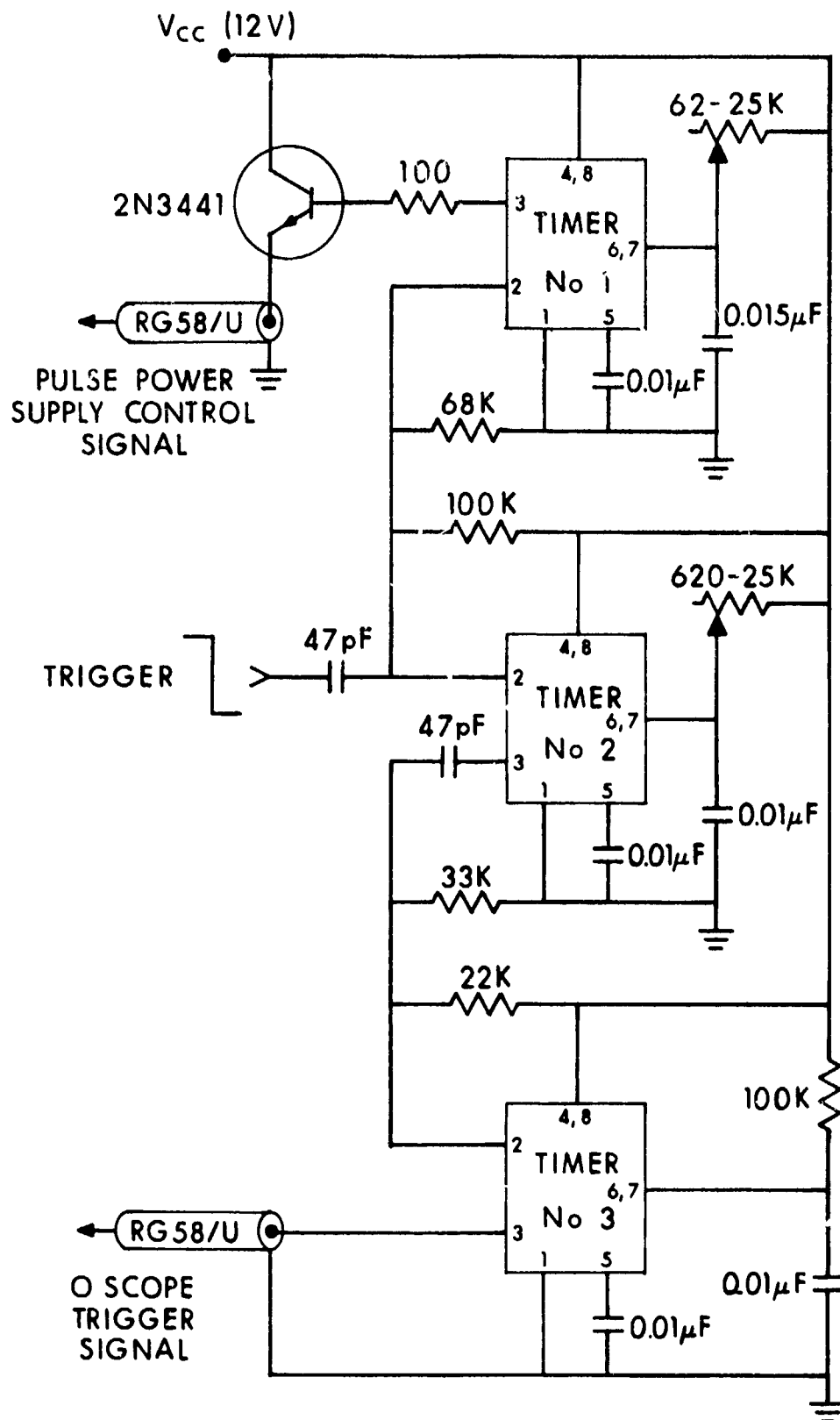
Figure 5. Schematic Diagram of Control Circuit for Pulse Power
Supplies and Oscilloscopes.

16

used as the gage factor (G.F.) in the well-known expression $\Delta R/R_o = G.F. \epsilon$
relating resistance change and strain. The usual convention of positive
tensile and negative compressive strain is followed. The gage manufacturer
suggests,[9] and independent tests confirm,[10] that this non-linear gage factor
is correct for large strain. Thus, gage resistance may vary unidirectionally
down to 76.8 ohms and up to 172.8 ohms from 120.0 ohms. Under these
conditions, bridge load range is 152.2 to 222.6 ohms. These values are used
as the maximum load excursions affecting excitation voltage stability.

A. Excitation Voltage Stability

Two factors affect excitation voltage stability: a) the exponential
voltage decay of the discharging capacitor, and b) the variation of
collector-emitter voltage across the switching transistor as collector current
changes. The measurement of compressive strains compounds these two factors
because as bridge load decreases, current requirements increase, which
hastens voltage decay and increases collector-emitter voltage. The first
factor is easily determined, the second depends on the output characteristics
of the transistor type, which must be measured.

The base current available is 7.5 milliamperes and Figure 6 shows
collector current, I_C vs collector-emitter voltage, E_{CE}. A decade resistance
box was the load, the capacitor charged to 36 volts, and pulse duration was
100 microseconds for these measurements. Differential amplifiers were used to
simultaneously measure E_{CE} and the voltage across the load. The output
characteristic curve shows that the transistor conducts with low forward
impedance (1.0 to 4.4 ohms) over the range of 20 to 210 milliamperes. Note
that this impedance variation destroys the gage cable termination by less than
five percent. The combination of excitation voltage and bridge load, to
include maximum excursions, however, should be such that I_C is within this
range. Also shown in Figure 6, as the right hand ordinate, is the excitation
voltage applied across a 185 ohm balanced bridge load corresponding to the
collector current indicated.

Hauver and Melani[4] report that total recording times of 150 microseconds
are required to completely record the strain-time histories of some impact
experiments. This, in addition to the 30 microseconds required for stabili-
zation of the power supply and bridge circuit after turn-on, necessitates a
minimum pulse width of 180 microseconds. Table 1 tabulates the range of
operation to allow this pulse width for several common zener diode voltages.
The allowable ranges are calculated by limiting the change in E_{CE} plus the
voltage decay over the pulse width indicated to less than or equal to 0.4
percent of the excitation voltage. The measurement of tensile strains
presents no limitations to the desired limit of 20 percent because the two

[9] *Measurements Group, Inc., High Elongation Strain Measurements, Technical Tip
No. TT-605, Raleigh, NC, 1983.*

[10] *R. E. Franz, "The Measurement of Large Strains with Foil Resistance Strain
Gages," Ballistic Research Laboratory Technical Report No. ARBRL-TR-02519,
August 1983. ADA 133 687*
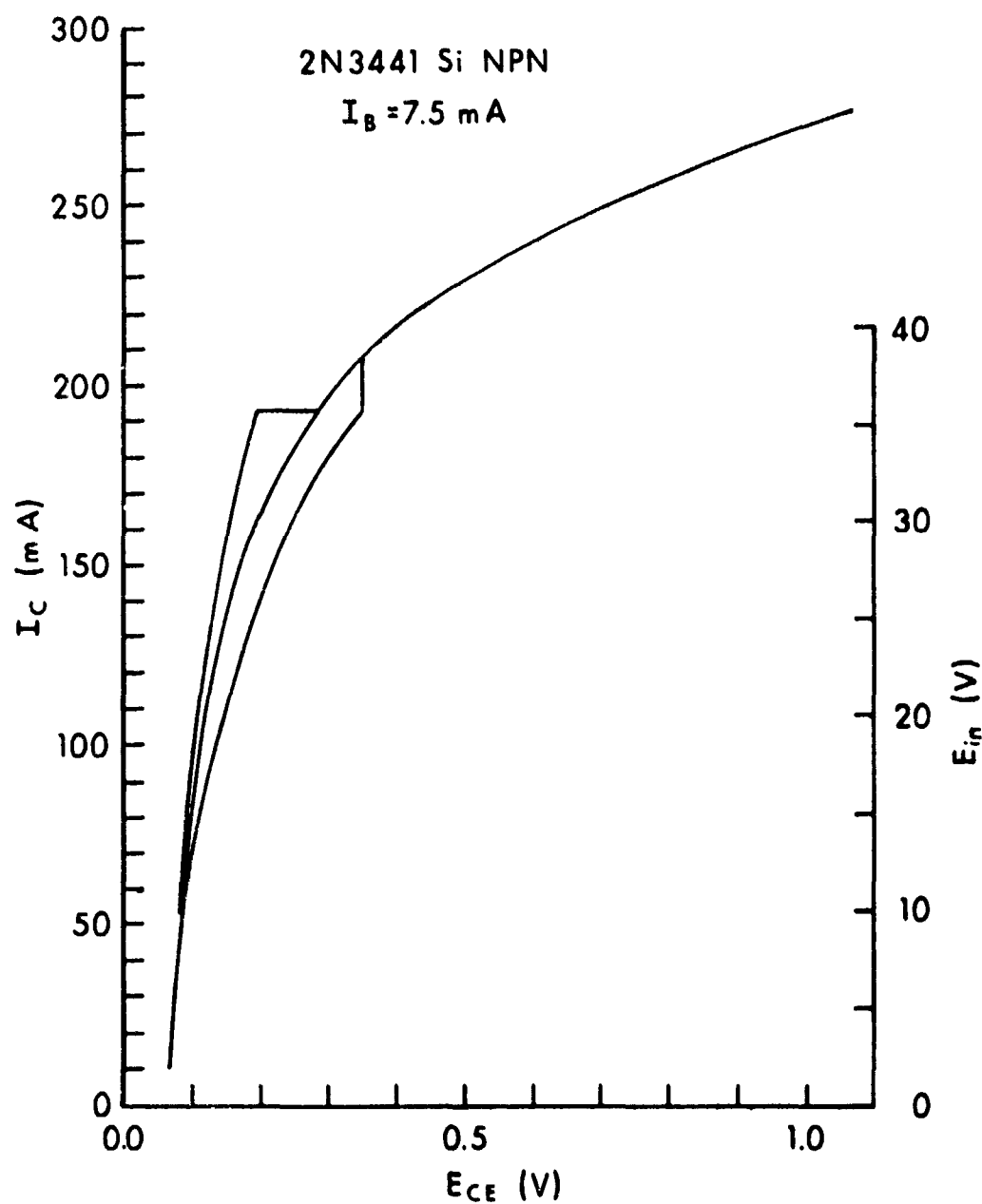
Figure 6. Output Characteristic of Switching Transistor. The envelope
indicates the permissable variation of collector current and
collector-emitter voltage for the excitation voltages given by
the right hand ordinate.

18

TABLE 1. RANGE OF OPERATION OF POWER SUPPLY AND BRIDGE

Nom. Zener Voltage (v)	I_C^a (mA)	E_{CE}^a (v)	Allowable Ranges			Max. Pulse Width (μs) @ Max. I_C
			I_C (mA)	R_g (Ω)	ϵ (+/− %)	
10	53.59	0.085	44.15 − 65.13	172.8 − 76.8	20 / 20	243
12	64.38	0.090	53.51 − 78.23	172.8 − 76.8	20 / 20	236
14	75.16	0.096	62.47 − 91.33	172.8 − 76.8	20 / 20	245
15	80.55	0.097	66.95 − 97.88	172.8 − 76.8	20 / 20	224
16	85.93	0.102	71.43 − 104.43	172.8 − 76.8	20 / 20	219
18	96.70	0.109	80.38 − 117.52	172.8 − 76.8	20 / 20	202
20	107.46	0.120	89.32 − 130.59	172.8 − 76.8	20 / 20	196
22	118.21	0.131	98.25 − 143.65	172.8 − 76.8	20 / 20	182
24	128.96	0.143	107.18 − 153.65	172.8 − 80.7	20 / 18	185
27	145.05	0.166	120.56 − 167.80	172.8 − 86.7	20 / 15	186
30	161.12	0.193	133.92 − 180.99	172.8 − 92.9	20 / 12	182
33	177.14	0.230	147.23 − 193.23	172.8 − 99.4	20 / 9	180
36	193.04	0.288	160.45 − 208.51	172.8 − 101.6	20 / 8	180

aConditions for 185 ohm balanced bridge load

19

factors affecting voltage stability tend to negate each other. The use of excitation above 22 volts, however, places some restriction on the magnitude of compresive strains which can measured and still insure excitation voltage stability. The allowable ranges of collector current and collector-emitter voltage lie within the envelope surrounding the characteristic curve in Figure 6.

B. Response Time

The turn-on response time of the power supply and bridge circuit determines the usable window of the pulse width, and is taken as the time required for excitation voltage and/or bridge output to reach its steady state value under constant load, whichever is longer. Figure 7a shows the control signal to the photodiode used to switch the power supply on and off. The 10.32 volt signal has a rise time of less than 100 nanoseconds and a pulse width of 198.75 microseconds. Also shown is the point at which the control circuit triggers the oscilloscopes in normal operation, 30 microseconds after control signal turn-on. The input signal to the control circuit (Figure 5) was used as the trigger in these tests, and this is taken as zero time. The bridge was statically balanced by applying five volts continuous DC excitation while monitoring output with a microvolt null detector.

The excitation and output voltage waveforms (Figure 7b and 7c) using a 15 volt zener diode (capacitor voltage 14.470) show mid-pulse excitation voltage was 14.355 volts and was within ± 0.4 percent of this value from 29.5 to 219.5 microseconds. The output voltage was 0.0 ± 0.8 mV (the minimum resolvable) from 21.0 to 241.0 microseconds. The usable window is determined by excitation voltage stability and the response time is 29.5 microseconds. A similar test using a 30 volt zener diode (capacitor voltage 28.530) shows mid-pulse excitation was 28.200 volts and met the stability criterion from 21.5 to 212.0 microseconds (Figure 7d), and output voltage was stable from 26.5 to 227.0 microseconds (Figure 7e). Here, the usable window is determined by output voltage stability. In both cases, however, the 30 microsecond pre-trigger is adequate time for the device to stabilize. Note that the excitation for both voltages remains on longer than the control signal. This is due to the capacitor in the switching transistor base circuit sourcing current after control signal turn-off, and transistor storage time. The true usable window of pulse width is, however, 30 microseconds after control signal turn-on to control signal turn-off.

The over-/undershoots of the bridge output voltages are due to the excitation voltage slewing rates acting upon reactances in the bridge load, and not due to the absolute magnitude of excitation because balanced bridge output is independent of excitation magnitude. Note that the peaks coincide with the steepest portions of the excitation voltage waveforms, i.e.,at the highest slewing rates, and that the magnitude of the peaks increases with excitation voltage. These magnitudes of approximately 20 millivolts should not overdrive an amplifier; however, "hard" turn-on of the power supply with 36 volt excitation produces an undershoot of 110 millivolts, which could be detrimental. In contrast, hard turn-on of a balanced bridge in which no coaxial cable is used produces an overshoot of only 7 millivolts. Thus the cable is the most reactive element of the bridge, and very long cables may severely degrade overall performance.
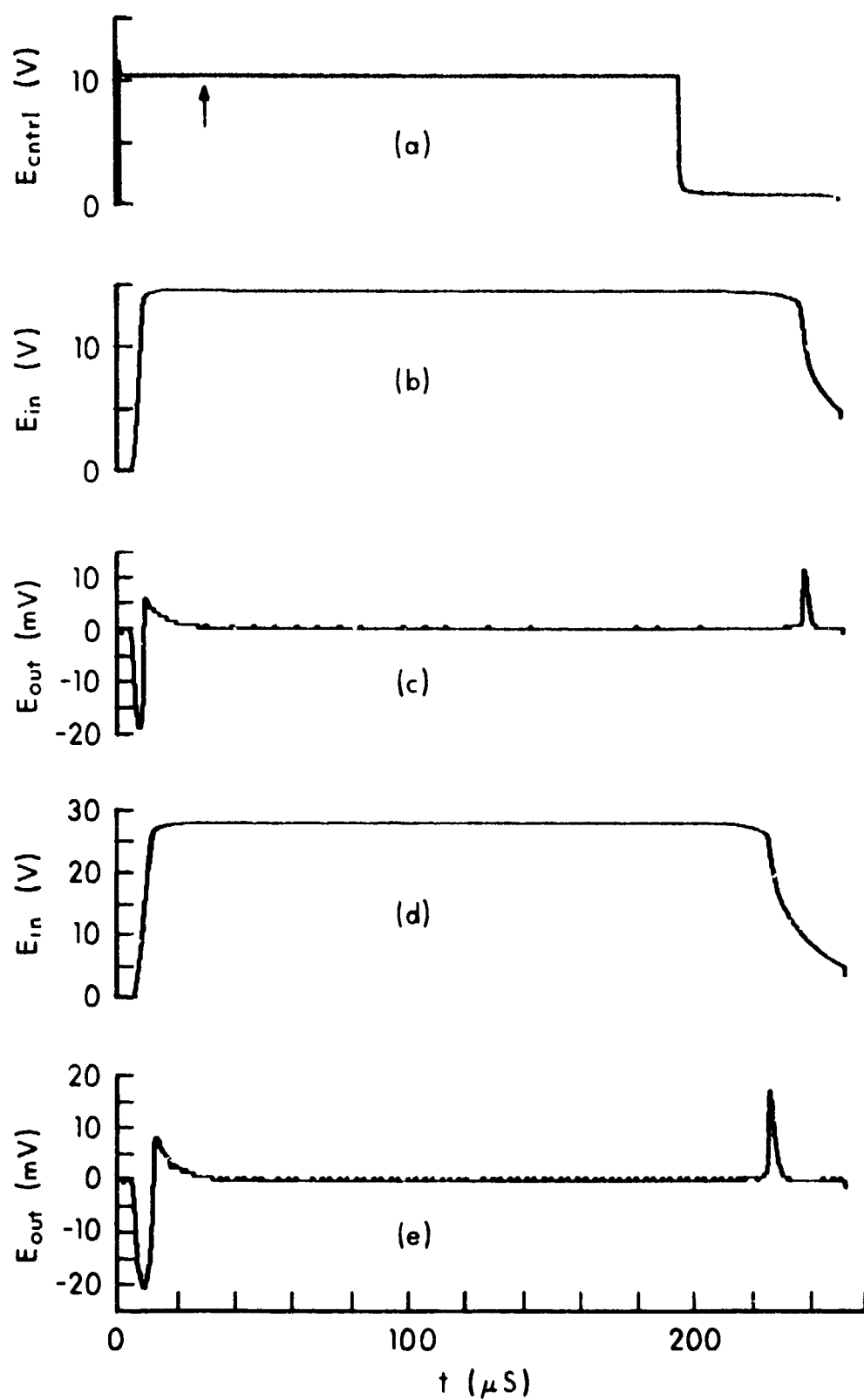
Figure 7. (a) Pulse Duration Control Signal, (b) Excitation and (c) Bridge Output Voltage, 15 Volt Zener Diode; (d) Excitation and (e) Bridge Output Voltage, 30 Volt Zener Diode, vs Time.

The slewing rate of current in the bridge which causes reactance induced instabilities to occur in the output can be used to estimate the strain-rate response characteristics of the bridge circuit. For this determination, an instability is defined as an induced voltage greater than the input noise level departing from the steady state condition. Specifically, this is an output of greater than 0.8 millivolts departing from the null balanced output.

Current in the gage arm of a balanced bridge is given by

$$I_g = E_{in} \Big/ (R_g + R_x + R_4) \qquad (6)$$

and slewing rate by

$$\dot{I}_g = -E_{in} \frac{(\dot{R}_g + \overset{o}{R}_x + \dot{R}_4)}{(R_g + R_x + R_4)^2} + \frac{\dot{E}_{in}}{R_g + R_x + R_4} \qquad (7)$$

In the tests illustrated in Figure 7, all derivatives of resistance with respect to time are zero, and $\dot{E}_{in}$ was $\pm$ 0.23v/μs at the onset of output instability for both voltages investigated. Thus the maximum magnitude of $\dot{I}_g$ is 1.067 x 10^3 A/s. During the usable window of the pulse width, the second term of Eq. 7 is on the order of unity, and thus is negligible. During dynamic straining, only $\dot{R}_g$ is non-zero, and this term can be expressed in terms of strain rate, $\dot{\epsilon}$ by differentiating Eq. 5. The maximum apparent strain rates to which the bridge can faithfully respond in terms of both strain and strain rate is given by

$$\left| \dot{\epsilon}_{max} \right| = \frac{\left| \dot{I}_g \right|_{max} (R_g + R_x + R_4)^2}{2E_{in}(R_g R_o)^{\frac{1}{2}}} \qquad (8)$$

where $\left| \dot{I}g \right|_{max}$ is experimentally determined for a given type bridge and cable design. Higher excitation voltages and increased bridge sensitivities tend to degrade strain rate response capabilities. Because bridge sensitivity is

22

non-linear for a quarter-bridge arrangement, the rate response characteristics are a function of the level of strain also, being less for compressive strains and greater for tensile strains, than the zero-strain value. The apparatus described here should respond to apparent strain rates of 10^4 s^{-1} at 20 percent compressive strain, provided excitation is 16.5 volts or less.

The position of the gage arm in the bridge is such that excessive real strain rates will cause bridge output to indicate greater resistance changes than have actually occurred due to strain. Apparent strain rates, as determined from the slopes of strain vs time records, will also be in error. If these apparent strain rates are greater than those determined to be acceptable by Eq. 8, the data analyst should suspect that errors in strain magnitude are also present. Apparent strain rates are always less than real strain rates, however, because of gage length resolution.

IV. CALIBRATION AND DATA REDUCTION

Raw, time resolved strain data for each gage is obtained by Eq. 9

$$\varepsilon(t) = \sqrt{R_g(t)/R_o} - 1 \qquad \cdot \tag{9}$$

These can be further reduced by correcting for angular misalignment of the gage axis with the intended axis of measurement,[11] transverse sensitivity,[12] and applying the appropriate rosette analysis, all of which are beyond the scope of the present report. R_o is measured directly using a digital multimeter in four terminal resistance modes; R_g is determined by using measured bridge output voltages in an algebraically manipulated form of Eq. 1. Circuit constants must be either directly measured or calculated based on calibration data. Two assumptions are made in reducing both the calibration and test data: 1) the excitation voltage is constant over the measurement window, that is, variation of E_{in} with respect to resistance and time is negligible, and 2) that bridge balancing sensitivity and output voltage resolution are such that the bridge may not be initially perfectly balanced. Both assumptions are supported by the performance test data.

Calibration data are obtained for each power supply/bridge circuit by measuring bridge output voltages for three known resistances of R_1: R_{1B}, R_{1C}

[11] Measurements Group, Inc., *Errors Due to Misalignment of Strain Gages*, Technical Note No. TN-511, Raleigh, NC, 1983.

[12] Measurements Group, Inc., *Errors Due to Transverse Sensitivity in Strain Gages*, Technical Note No. TN-509, Raleigh, NC, 1982.

and R_{1T}. All three include the gage cable and lead resistance, R_x; the first includes the gage (R_o) only, while the remaining two have precision metal film resistors in parallel and series, respectively, with the gage. The resistors are chosen to create nearly equal voltage excursions from that obtained with the gage only, which is at or near balance, although it need not be so. Also, the calibration voltages are greater than 80 percent of full scale on the most sensitive range of the oscilloscope to minimize relative uncertainty. All R_1 and bridge resistor R_4 are measured in the same manner as R_o.

Let E_B, E_C and E_T be the bridge output voltages measured at mid-usable pulse width, obtained with measured resistances R_{1B}, R_{1C} and R_{1T}, respectively, comprising the gage arm resistance. Let the second term in parentheses of Eq. 1, $R_2/(R_2 + R_3)$, be the balance ratio, R_{bal}, calculated by

$$R_{bal} = \frac{E_T\left(\dfrac{R_{1C}}{R_{1C} + R_4}\right) - E_C\left(\dfrac{R_{1T}}{R_{1T} + R_4}\right)}{E_T - E_C} \ . \tag{10}$$

The excitation voltage, E_{in} is given by

$$E_{in} = \frac{E_T}{\dfrac{R_{1T}}{R_{1T} + R_4} - R_{bal}} = \frac{E_C}{\dfrac{R_{1C}}{R_{1C} + R} - R_{bal}} \ . \tag{11}$$

The actual zero-strain output voltage may be calculated by

$$E_{base} = E_{in}\left(\frac{R_{1B}}{R_{1B} + R_4} - R_{bal}\right) \tag{12}$$

and compared with E_B as a crosscheck; the difference between the two should be less than the minimum resolution. The non-linear relationship between R_1 and bridge output voltage requires calculation of a resistance offset given by

$$R_{offset} = R_{1B} - R_{dum} \tag{13}$$

where R_{dum} is

$$R_{dum} = \frac{R_{bal}}{1 - R_{bal}} R_4 \quad . \tag{14}$$

This is, in effect, a dummy resistance that R_1 would have to be to have true balance with the current balance ratio. Equations 10 thru 14 provide the circuit constants needed for data reduction.

If $E_s(t)$ is the bridge output voltage during straining, a quantity $X(t)$ is given by

$$X(t) = \frac{E_s(t) - E_{base}}{E_{in}} + R_{bal} \tag{15}$$

and gage arm resistance is

$$R_1(t) = \frac{X(t)}{1 - X(t)} R_4 + R_{offset} \quad . \tag{16}$$

Gage resistance for use in Eq. 9, $R_g(t)$ is obtained by subtracting the lead resistance R_X from the result of Eq. 16.

An assessment of the uncertainty and overall accuracy of the strain measurements made with this apparatus was made. The resistances R measured with the digital multimeter are accurate to $\pm$ (0.002 percent R + 4 milliohms), with one milliohm resolution. Calibration and strain signal voltages measured with an 8-bit digital storage oscilloscope arc accurate to $\pm$ 0.5 percent of full scale, with 0.8 millivolt resolution. A rigorous mathematical treatment of the uncertainties associated with the measured quantities in Eqs. 9 thru 16 provides an estimate of the external error associated with the strain measurement.[13] Using 15 volts as a nominal excitation, strain data are accurate to $\pm$ (1.4 percent ∈ + 375 microstrain), with 110 microstrain resolution. Increasing the excitation voltage improves resolution (up to the balancing sensitivity of 45 microstrain with 36 volts); however, overall accuracy remains essentially the same. Appendix C contains a sample calibration and

[13]N. Cook and E. Rabinowitz, *Physical Measurement and Analysis*, Addison-Wesley Publishing Co., Reading, 1963, pp. 29-35.

data reduction and shows the accuracy is actually on the order of the resolution of the measurement scale.

V. SUMMARY

A pulsed power supply and Wheatstone bridge circuit for measuring large, high strain rate strains with foil type resistance strain gages has been designed, constructed and evaluated for overall performance. The unit has a signal to noise ratio up to six times better than conventional strain gage signal conditioning equipment and can be used to measure static strains by discrete sampling or dynamic strains at rates up to 10^4 s^{-1} over a sample time of 35 to 200 microseconds. Strains to ± 20 percent can be measured with an overall accuracy of ± (1.4 percent ϵ + 375 microstrain). The compact, self-contained unit (10.5cm L x 6.0cm W x 8.0cm H, 250g) shown in Figure 8 connects directly to an oscilloscope, and a simple trigger control circuit, also described herein, is the only additional equipment required. Thus, the unit is well suited for field testing, as well as laboratory applications. The complete design specifications included allow the unit to be adapted for use with other types of resistive element transducers, such as pressure gages and temperature sensors.
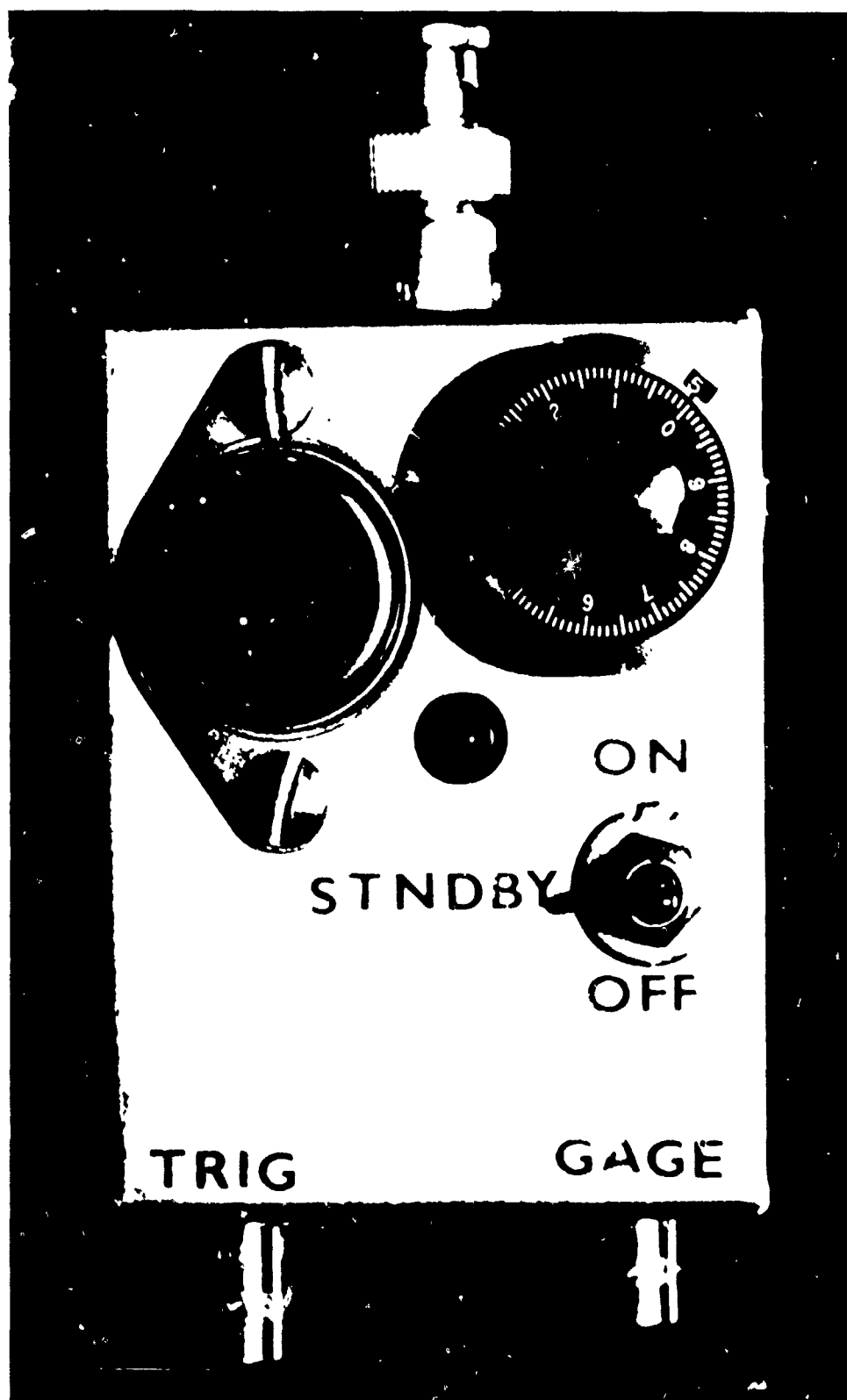
Figure 8. Self-Contained Pulse Power Supply and Bridge. The BNC plug permits direct connection to an oscilloscope. Both the power supply and switch batteries are mounted on the bottom of the device.

ACKNOWLEDGMENT

REFERENCES

1. Ralph Morrison, Grounding and Shielding Techniques in Instrumentation, 2nd ed., John Wiley and Sons, Inc., New York, Chichester, Brisbane, Toronto, 1977.

2. Measurements Group, Inc., Optimizing Strain Gage Excitation Levels, Technical Note No. TN-502, Raleigh, NC, 1979.

3. W. N. Sharpe, Jr., "Dynamic Plastic Response of Foil Gages," Experimental Mechanics, Vol. 10, No. 10, October 1970, pp. 408-414.

4. G. E. Hauver and A. Melani, "Strain-Gage Techniques for Studies of Projectile Behavior During Penetration," Ballistic Research Laboratory Memorandum Report No. ARBRL-MR-03082, February 1981. ADA 098660

5. C. C. Perry and H. R. Lissner, The Strain Gage Primer, McGraw-Hill Book Co., Inc., New York, Toronto, London, 1955, pp. 48-51.

6. Radio Corporation of America, Inc., Power Transistors, Databook No. SSD-204C, Somerville, NJ, 1974, pp. 109-115.

7. Texas Instruments, Inc., The Optoelectronics Data Book for Design Engineers, 5th ed., Dallas, TX, 1978, pp. 114-118.

8. Motorola, Inc., Linear Integrated Circuits, Series C, Phoenix, AZ, 1979, pp. 6-44 - 6-50.

9. Measurements Group, Inc., High Elongation Strain Measurements, Technical Tip No. TT-605, Raleigh, NC, 1983.

10. R. E. Franz, "The Measurement of Large Strains with Foil Resistance Strain Gages," Ballistic Research Laboratory Technical Report No. ARBRL-TR-02519, August 1983. ADA 133687

11. Measurements Group, Inc., Errors Due to Misalignment of Strain Gages, Technical Note No. TN-511, Raleigh, NC, 1983.

12. Measurements Group, Inc., Errors Due to Transverse Sensitivity in Strain Gages, Technical Note No. TN-509, Raleigh, NC, 1982.

13. N. Cook and E. Rabinowitz, Physical Measurement and Analysis, Addison-Wesley Publishing Co., Reading, 1963, pp. 29-35.

A-1. Measurements Group, Inc., Temperature Induced Apparent Strain and Gage Factor Variation in Strain Gages, Technical Note No. TN-504, Raleigh, NC, 1976.

B-1. D. F. Merritt and C. E. Anderson, Jr., "X-Ray Trigger Predictor: Automatic Electronic Time Delay Device for Flash X-Ray Systems," Ballistic Research Laboratory Technical Report No. ARBRL-TR-02284, January 1981. ADB 056362

APPENDIX A

OPTIMIZING PULSE EXCITATION LEVELS

FOR CONSTANTAN FOIL STRAIN GAGES

APPENDIX A

OPTIMIZING PULSE EXCITATION LEVELS FOR CONSTANTAN FOIL STRAIN GAGES

The Measurements Group, Inc., publication, Optimizing Strain Gage Excitation Levels,[2] provides an excellent summary of the factors affecting choice of excitation level for strain gages, and includes recommended power density ranges based on the level of accuracy required and the heat sinking capability of the substrate to which the gage is bonded. The recommended power densities are for conti"uous excitation, however, and are intended to minimize zero-shift due to apparent strain within the level of accuracy stated.

Apparent strain is a temperature induced change of gage resistance, and under equilibrium temperature conditions, errors due to apparent strain can be corrected.[A-1] During pulse excitation, however, thermal equilibrium between the grid material and the substrate is not achieved due to the low thermal conductivity of the gage backing. Consequently, the grid material is heated, but cannot expand in the plane of the gage. It may expand out-of-plane, however, effectively increasing the cross-sectional area of the grid. Since the resistance R(ohms) of a conductor is given by

$$R = \rho L/A \qquad\qquad (A-1)$$

where
   A - cross-sectional area, cm^2
   L - length, cm
   ρ - resistivity, ohm-cm

increasing A causes resistance to decrease. Thus, compressive apparent strain is indicated when the grid becomes heated.

Power density is a convenient parameter when discussing strain gage excitation levels because it takes into account variations in instrumentation design and gage geometry, as well as excitation voltage. The power to be dissipated in the gage grid is $I_g^2 R_g$, where I_g is the current passing thru the gage, Eq. 6. Power density is simply this power divided by the active area (gage length x grid width) of the gage. Apparent strain zero-shift may be calculated from bridge output voltage zero-shift.

Tests were performed on annealed constantan foil strain gages to determine apparent strain zero-shift vs pulsed power density. The specific gage tested was a Micro-Measurements EP-08-062AK-120, bonded with methyl-2-cyanoacrylate to a 1.2 mm wall, 24.7 mm O.D. AISI 1020 steel tube. A 0.025 mm polyurethane protective coating was applied over the installation, in accordance with the gage manufacturers recommendations. The steel substrate was chosen as

---

[A-1] Measurements Group, Inc., *Temperature Induced Apparent Strain and Gage Factor Variation in Strain Gages*, Technical Note No. TN-504, Raleigh, NC, 1976.
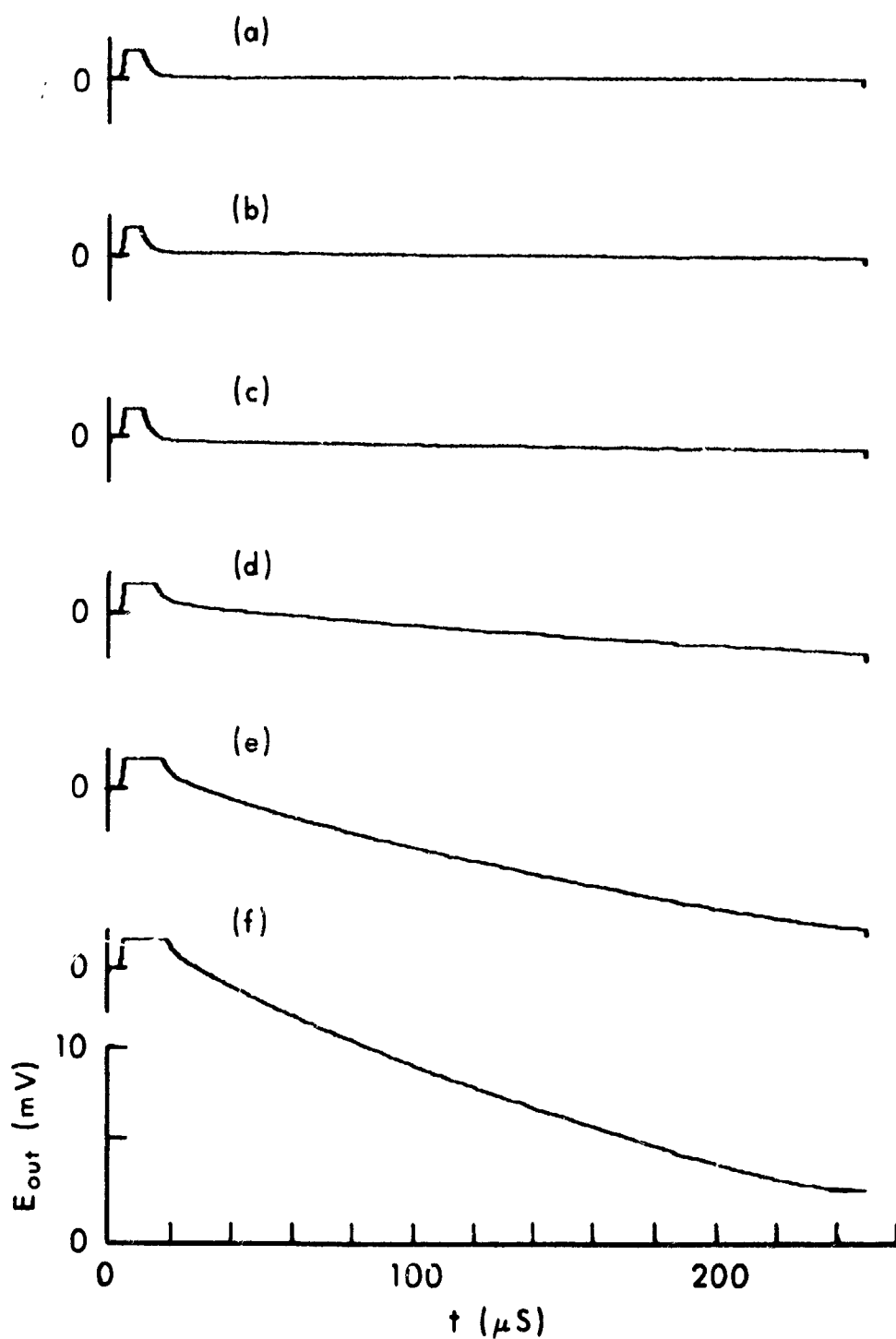
Figure A-1. Zero-Shift vs Excitation Time. (a) Reference Baseline, 5 W Metal Film Resistor as Gage Substitute. Power Densities of (b) 0.1107, (c) 0.2038, (d) 0.6526, (e) 1.3490 and (f) 1.8381 W/mm^2 in Annealed Constantan Foil Strain Gage Mounted on Steel.

typical, and has "good" heat sink capability. The gage was connected to a pulse power supply/Wheatstone bridge circuit of the type described in this report with 25 cm of RG-62/U coaxial cable. Zener diodes ranging from 10 to 43 volts regulated excitation voltage, which was pulsed on for 200 microseconds. Actual pulsed excitation voltages across the bridge were measured directly to ± 5 millivolt accuracy, while bridge output voltages were measured to ± 50 microvolt accuracy.

Zero-shift vs excitation time for several power densities is shown in Figure A-1. After the 30 microseconds required for circuit stabilization, zero-shift increases at nearly constant rate for each power density, and the rate of zero-shift increases with power density. The rate of zero-shift does decrease somewhat with time, however, as heat generated in the grid is conducted to the substrate. This, of course, occurs more rapidly for higher grid temperatures. It is expected that for very long excitation times, the zero-shift would stabilize as the grid reached thermal equilibrium.

The rate of zero-shift was assumed constant, and the data reduced to apparent microstrain per microsecond of excitation using Eqs. 15, 16, and 9, and assuming initial balance. These zero-shift rates are plotted vs power density in Figure A-2, and the error bars indicate the uncertainty. A linear least squares fit was performed on the data, and the result is the solid line. Of interest is the intersection of the line with the power density axis, 0.0568 W/mm^2, corresponding to zero zero-shift rate, and hence, no zero-shift. This is in the range of 0.031 - 0.078 W/mm^2, indicated on the figure, recommended by the gage manufacturer as the maximum continuous power densities.[2]

To use the curve for estimating optimum pulse excitation levels, the allowable zero-shift rate must be determined. This is the strain measurement resolution divided by total excitation time, $\mu\epsilon/\mu s$. The power density can then be read from the curve, and excitation voltage calculated by Eq. 4. The measurement resolution using this excitation should be re-evaluated to determine if the power density is acceptable. A word of caution concerning use of this curve is in order. The data were obtained using short (200 microsecond) pulse widths, good substrate heat sink capability and a strain gage with 08 self-temperature compensation (S-T-C). (Thermal coefficient of expansion 8 ppm/°F (14.4 ppm/°C).) For much longer pulse widths, the rate of zero-shift may be inversely proportional to substrate thermal conductivity. The S-T-C number also affects the slope of the line in Figure A-2. Lower thermal expansion coefficients (S-T-C number) allow greater power densities for a given zero-shift rate and vice versa. Because quarter bridge output and the strain reduction used are both non-linear, extrapolation to much higher power densities is not recommended without verification of applicability.
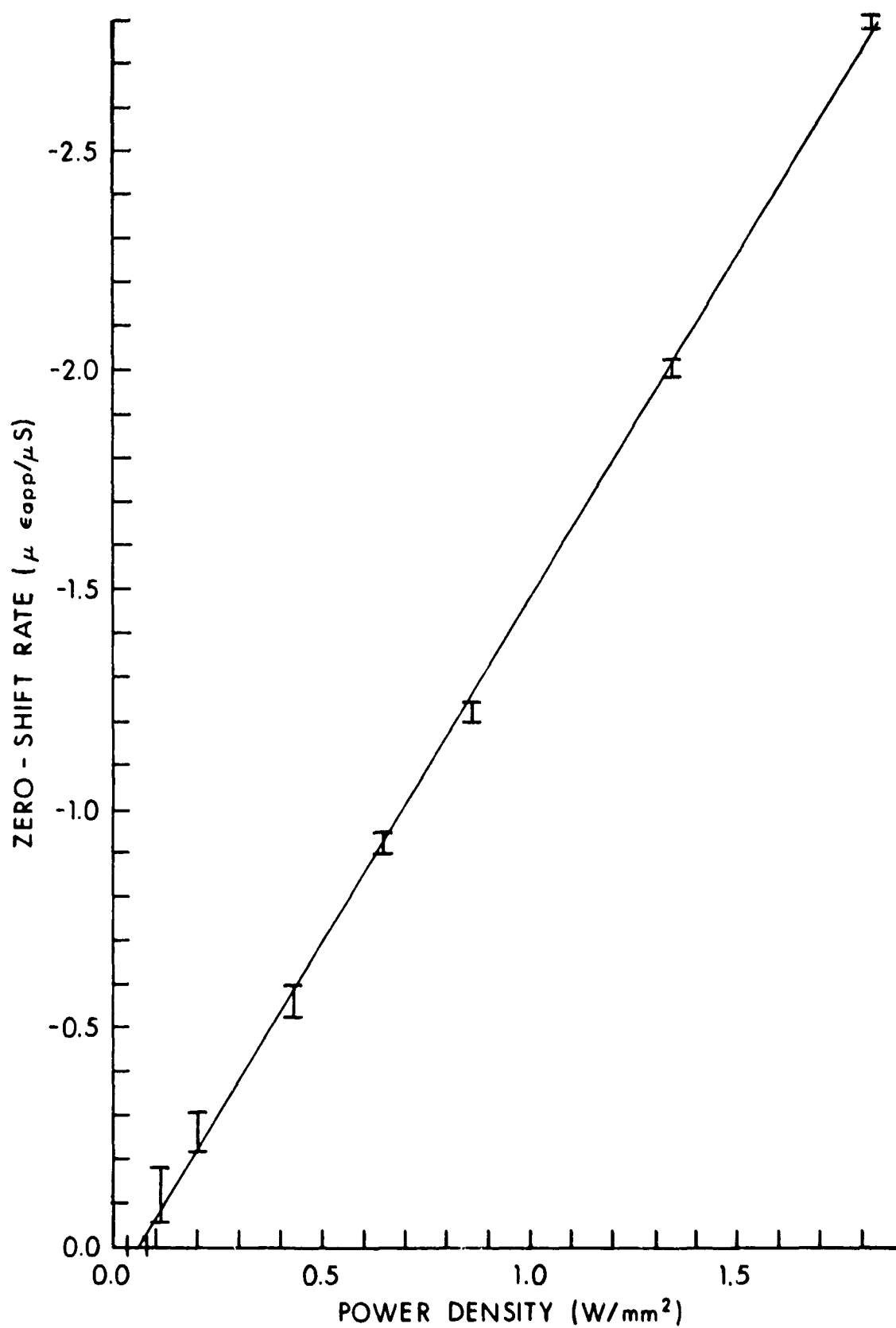
Figure A-2. Apparent Strain Zero-Shift Rate vs Pulsed Power Density for Annealed Constantan Foil Strain Gage.

36

APPENDIX B

TIME DOMAIN PRE-EVENT TRIGGER FOR

CONSTANT VELOCITY IMPACT

SYSTEMS

APPENDIX B

TIME DOMAIN PRE-EVENT TRIGGER FOR CONSTANT VELOCITY IMPACT SYSTEMS

The acquisition of transient experimental data requires precise triggering of instrumentation to insure recording the events of interest. An automatic, electronic time delay trigger device, developed by Merritt and Anderson,[B-1] is useful in impact studies because it provides a trigger at or just before impact. The device is a TTL up/down counter, and operates in this manner. Two passive circuits that detect the passage of a projectile or fragment are spaced a distance X along the projectile's line of flight, the second a distance 2X from the target. When the projectile arrives at the first circuit, the counter starts incrementing one count for each pulse provided by a 1 MHz oscillator. Upon projectile arrival at the second circuit, the counter stops incrementing, and starts decrementing one count for each two 1 MHz pulses. Thus, it takes the counter twice the time to decrement to zero as it did to count up. A projectile travelling at constant velocity will take twice the time to travel a distance 2X as it does to travel 1X, so it will reach the target at the same time the counter returns to zero. A comparator circuit detects the return to zero and outputs a trigger pulse.

The developers state that spacing the target 'slightly' greater than twice the inter-detection-circuit spacing from the second circuit will provide a trigger before impact. This is space domain pre-event triggering, and the amount of time before the event depends on the amount of this 'slightly' greater spacing and the projectile velocity. If time domain pre-event triggering is required, as for example to allow pulsed instrumentation to stabilize, either the velocity must be known beforehand to calculate the distance, or an alternative device must be developed. This appendix describes a modification to the original trigger predictor circuit to allow time domain pre-event triggering.

Merritt and Anderson provide an excellent description of the detailed operation of the device, and the reader is directed to their report. The entire circuit diagram, Figure B-1, with the modification is included here, however, for clarity and completeness, and Table B-1 lists the integrated circuits used.

In the original design, the 12 bit binary counter, IC8, 9 and 10, has each output register Q connected to an inverter, IC6A-F and IC7A-F. The inverter outputs, which are open collector, are all tied together and to a single 1 K-ohm pull up resistor. When any counter register is in the high logic level state, i.e., counter not at zero, the corresponding inverter output is in the low logic level state, and the pull up current is sunk to ground. So output of the paralleled inverters is high only when all counter registers are zero. The low to high transition when the counter decrements to zero triggers a monostable multivibrator, (not shown in schematic) which provides a trigger pulse. Also, an output to reset the STOP flip-flop, IC1A, to prevent decrementing past zero is provided to prevent subsequent retriggering.

[B-1] D. F. Merritt and C. E. Anderson, Jr., "X-Ray Trigger Predictor: Automatic Electronic Time Delay Device for Flash X-Ray Systems," Ballistic Research Laboratory Technical Report No. ARBRL-TR-02284, January 1981. ADB 056362

Figure B-1.   Schematic Diagram of Time Domain Pre-Event Trigger Circuit.

40
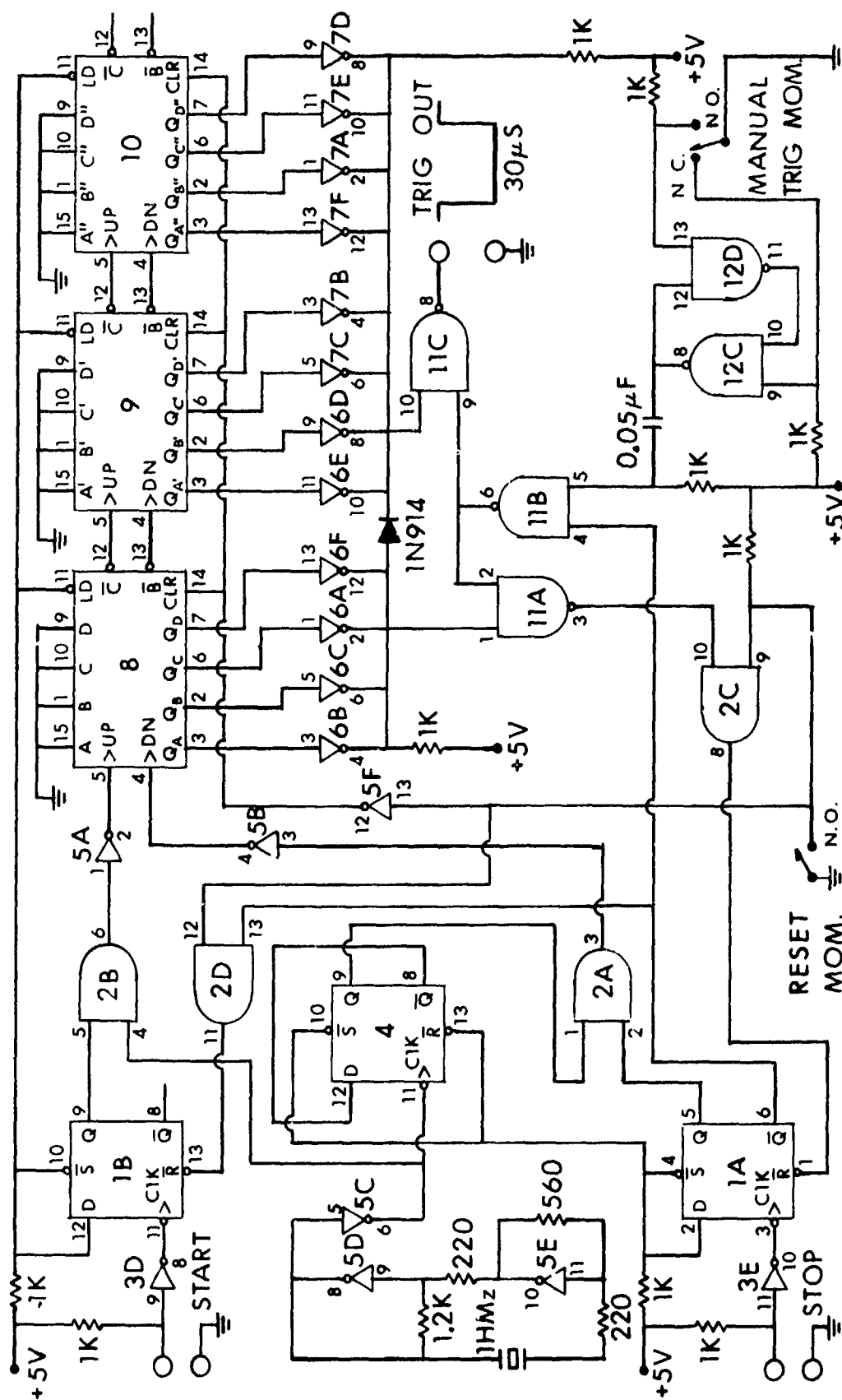
TABLE B-1. ICs USED IN PRE-EVENT TRIGGER DEVICE

IC No.	Type No.	Function
1A-B,4	SN7474	D-type, positive edge triggered flip-flop
2A-D	SN7408	2-input positive AND gate, totem pole output
3D-E, 5A-F	SN7404	Inverter, totem pole output
6A-F, 7A-F	SN7405	Inverter, open collector output
8,9,10	SN74193	Positive edge triggered, 4-bit binary up/down synchronous counter
11A-C, 12C-D	SN7400	2-input positive NAND gate, totem pole output

The modification involves splitting the inverter outputs with a diode and providing pull up current to both parallel inverter circuits thru 1 K-ohm resistors. Current cannot flow cathode to anode, so when the counter registers corresponding to those inverters tied to the cathode side are zero, output is high regardless of the state of the registers on the anode side. Conversely, current may flow in the opposite direction, so output of the inverters tied to the anode is low when any register is high. Thus two outputs are available, one from the anode side when the counter has decremented to zero, and another from the cathode side. The time before zero that the cathode side goes high depends on the number of registers n tied to the anode side, and is given by

$$\sum_{i=1}^{n} 2^{i-1} \uparrow$$

(B-1)

where $\uparrow$ is the period of the oscillator providing decrement pulses. In this case n is 4 and $\uparrow$ is 2 microseconds, so pre-event time is 30 microseconds.

IC11A-C comprise the output section, replacing the monostable multivibrator in the original device. The output of IC11A is used to reset the STOP flip-flop in a fashion similar to the original version of the circuit. IC11C provides the pre-event trigger signal, a TTL level high to low transition. IC11B is used as a low active OR gate to enable output. One input, pin 5, is normally high, the other, pin 4, is low only when the STOP flip-flop has been triggered. Thus IC11A and IC11C are enabled only during decrementing of the counter.

41

The output may be manually triggered by momentarily causing pin 5 of IC11B to be low. This is done with the flip-flop switch comprised of IC12C and D and the resistance-capacitance circuit. The manual trigger can be used for pre-shot testing and calibration of other instrumentation.

To insure that the desired amount of pre-event time is obtained, the counter must increment to at least all registers associated with the anode side of the diode. The time is given by Eq. B-1, where $\wedge$ is the period of the increment pulses, 1 microsecond. The projectile velocity and detection circuit spacing must be such that 15 microseconds or more "count up" time is obtained. This is not a severe limitation unless velocity is very high or circuit spacing is very small. If this situation is not met, the circuit will still trigger, but the pre-event time will be only twice the count up time.

Timing accuracy of the device is limited by the asynchronicity of the START and STOP pulses with the oscillator pulses. Incrementing, the uncertainty is zero to +1 count and decrementing, zero to -1 count for a total uncertainty of ± 3 microseconds. Thus, the pre-event trigger can occur between 27 and 33 microseconds before impact. One hundred tests show the uncertainty is random, with a mean pre-event time of $30.1 \pm .1$ microseconds and a standard deviation of 1.5 microseconds. The uncertainty could be decreased by using a higher frequency oscillator, but this would necessitate additional counter bits to retain the counting capacity.

APPENDIX C

SAMPLE CALIBRATION AND STRAIN

DATA REDUCTION

APPENDIX C

SAMPLE CALIBRATION AND STRAIN DATA REDUCTION

A typical calibration and simulated strain data reduction was performed, with total pulse durations of 200 microseconds and the bridge output voltages measured at mid-usable-pulse-width, 115 microseconds after turn-on. The actual excitation voltages, not normally directly measured during calibration, were measured with an oscilloscope with a differential preamplifier for comparison with the calculated value. The most general case of the bridge being slightly unbalanced initially was used in the example. A five watt, 120 ohm metal film resistor was used as a gage substitute and connected to the bridge with 14 meters of RG-62/U coaxial cable. A nominal 15 volt zener diode regulated the excitation voltage. Table C-1 shows directly measured calibration resistances and bridge output voltages needed to calculate the circuit constants, as well as the measured excitation voltages. Table C-2 shows the calculated circuit constants based on the data of Table C-1. The calculated excitation and baseline bridge output voltages are in excellent agreement with the measured values.

To test the strain data reduction procedure, several compressive strain simulations were performed. Precision metal film resistors were inserted in parallel with the gage substitute to simulate a gage under strain, and the bridge output measured on several oscilloscope scales, each with different resolution, to test the validity of calibration on one scale and signal measurement on another. The resistance of the "gage under strain" was measured directly, and this value used to calculate the "actual strain." The "calculated strain" and uncertainty were determined from output voltage and resolution limit. The difference between the two determinations is the error. See Table C-3.

The error associated with these measurements is on the order of the resolution of the measurement scale. Calibrating on a high resolution scale provides more accurate circuit constants, and the scale may be changed to accommodate the expected range of measurement without loss of calibration.

TABLE C-1. MEASURED CALIBRATION CONSTANTS

R (Ω)	E_{out} (mv)	E_{in} (v)
R_o = 119.664	–	–
R_4 = 92.9686	–	–
R_{1B} = 122.274	E_B = –15.?	13.825
R_{1T} = 124.725	E_T = +52.0	13.835
R_{1C} = 119.880	E_C = –82.4	13.840

TABLE C-2. CALCULATED CIRCUIT CONSTANTS

R_x (Ω)	R_{bal} (Ω/Ω)	R_{dum} (Ω)	R_{offset} (Ω)	E_{in} (v)	E_{base} (mv)
2.610	0.56918	122.825	–0.551	13.826	–15.23

TABLE C-3. DATA REDUCTION AND COMPARISON WITH ACTUAL STRAIN

$E_s \pm$ res (mv)	$\epsilon_{calc} \pm$ res $(\mu\epsilon)$	act $(\mu\epsilon)$ [a]	Error $(\mu\epsilon)$
–50.4 ± 0.8 [b]	–5306 + 120	–5443	–137
–52.8 ± 1.6	–5667 ± 241	–5443	+224
–150.4 ± 1.6	–20211 ± 241	–20121	+90
–48 ± 16	–4945 ± 2406	–5443	–448
–144 ± 16	–19265 ± 2406	–20121	–856
–1488 ± 16	–198435 ± 2406	–198779	–344

[a] $^{+53}_{-}$

[b] Same scale and resolution as calibration measurements

46

DISTRIBUTION LIST

Copies	Organization
12	Administrator Defense Technical Info Center ATTN: DTIC-DDA Cameron Station Alexandria, VA 22314

2	Director
	Defense Advanced Research
	  Projects Agency
	ATTN: Tech Info
	      Dr. E. Van Reuth
	1400 Wilson Boulevard
	Arlington, VA 22209

1	Deputy Assistant Secretary of the Army (P&D) Department of the Army Washington, DC 20310
1	HQDA (DAMA- ARZ, Dr. Watson) Washington, DC 20310
1	HQDA (DAMA-MS) Washington, DC 20310
1	Commandant Command and General Staff College ATTN: Archives Fort Leavenworth, KS 66027
1	Commander US Army War College ATTN: Lib Carlisle Barracks, PA 17013
1	Commander US Army Materiel Development and Readiness Command ATTN: DRCDRA-ST 5001 Eisenhower Avenue Alexandria, VA 22333
1	HQDA DAMA-ART-M Washington, DC 20310
1	Commander US Army Development & Employment Agency ATTN: MODE-TED-SAB Fort Lewis, WA 98433

Copies	Organization

7	Commander
	Armament R&D Center
	US Army AMCCOM
	ATTN: DRSMC-LC(D), J. Frasier
	        DRSMC-LCA(D), T. Davidson
	        DRSMC-SC(D), J. D.Corrie
	                     J. Beetle
	                     E. Bloore
	        DRSMC-TDC(D)
	        DRSMC-TSS(D)
	Dover, NJ 07801

1	Director Benet Weapons Laboratory Armament R&D Center US Army AMCCOM ATTN: DRSMC-LCB-TL(D) Watervliet, NY 12189
1	Commander US Army Armament, Munitions and Chemical Command ATTN: DRSMC-LEP-L(R) Rock Island, IL 61299

6	Director
	Benet Weapons Laboratory
	Armament R&D Ctr, US Army AMCCOM
	        Dr. Julian Wu, Dr.M.A. Hussain
	        Dr. John Underwood
	        Mr. D. P. Kindall
	        Dr. J. Throup
	        Dr. E. Schneider
	Watervliet, NY 12189

1	Commander US Army Aviation Research and Development Command ATTN: DRDAV-E 4300 Goodfellow Boulevard St. Louis, MO 63120
1	Director US Army Air Mobility Research and Development Laboratory Ames Research Center Moffett Field, CA 94035

DISTRIBUTION LIST

Copies	Organization	Copies	Organization

1 Commander
US Army Communications Research
  and Development Command
ATTN: DRSEL-ATDD
Fort Monmouth, NJ 07703

1 Commander
US Army Electronics Research
  and Development Command
Technical Support Activity
ATTN: DELSD-L
Fort Monmouth, NJ 07703

1 Commander
US Army Harry Diamond Laboratory
ATTN: DELHD-TA-L
2800 Powder Mill Road
Adelphi, MD 20783

1 Commander
US Army Missile Command
ATTN: DRSMI-R
Redstone Arsenal, AL 35898

1 Commander
US Army Missile Command
ATTN: DRSMI-YDL
Redstone Arsenal, AL 35898

2 Commander
US Army Mobility Equipment
  Research & Development Command
ATTN: DRDME-WC
      DRSME-RZT
Fort Belvoir, VA 22060

3 Director
US Army BMD Advanced
  Technology Center
ATTN: ATC-T, M. Capps
      ATC-M, S. Brookway
      ATC-RN, P.Boyd
P. O. Box 1500, West Station
Huntsville, AL 35807

1 Commander
US Army Natick Research and
  Development Center
ATTN: DRDNA-DT, Dr. D. Sieling
Natick, MA 01762

1 Commander
US Army Tank Automotive Command
ATTN: DRSTA-TSL
Warren, MI 48090

1 Commander
US Army Electronics Proving
  Ground
ATTN: Tech Lib
Fort Huachuca, AZ 85613

3 Commander
US Army Materials and Mechanics
  Research Center
ATTN: DRXMR-T, J. Mescall
      DRXMR-T, R. Shea
      DRXMR-H, S. C. Chou
Watertown, MA 02172

5 Commander
US Army Research Office
ATTN: Dr. R. Weigle
      Dr. E. Saibel
      Dr. G. Mayer
      Dr. F. Smiedeshoff
      Dr. J. Chandra
P. O. Box 12211
Research Triangle Park, NC
27709

2 Commander
US Army Research and
  Standardization Group
  (Europe)
ATTN: Dr. B. Steverding
      Dr. F. Rothwarf
Box 65
FPO NY 09510

1 Director
US Army TRADOC Systems
  Analysis Activity
ATTN: ATAA-SL
White Sands Missile Range
NM 88002

1 Commandant
US Army Infantry School
ATTN: ATSH-CD-CSO-OR
Fort Benning, GA 31905

DISTRIBUTION LIST

Copies	Organization	Copies	Organization

2   Office of Naval Research
ATTN: Code 402
808 N. Quincy Street
Arlington, VA 22211

3   Commander
US Naval Air Systems Command
ATTN: AIR-604
Washington, DC 20360

1   Commander
Naval Ordnance Systems Command
Washington, DC 20360

3   Commander
Naval Surface Weapons Center
ATTN: Dr. W. H. Holt
       Dr. W. Mock
       Tech Lib
Dahlgren, VA 22448

3   Commander
Naval Surface Weapons Center
ATTN: Dr. R. Crowe
       Code R32, Dr. S.Fishman
       Tech Lib
Silver Spring, MD 20910

5   Commander
US Naval Research Laboratory
ATTN: C. Sanday
       R. J. Weimer
       Code 5270, F. MacDonald
       Code 2020, Tech Lib
       Code 7786, J. Baker
Washington, DC 20375

1   Director
Lawrence Livermore Laboratory
ATTN: Dr. M. L. Wilkins
P. O. Box 808
Livermore, CA 94550

7   Commander
Naval Research Laboratory
Engineering Materials Division
ATTN: E. A. Lange
       G. R. Yoder
       C. A. Griffis
       R. J. Goode
       R. W. Judy, Jr.
       A. M. Sullivan
       T. W. Crooker
Washington, DC 20375

1   AFWL/SUL
Kirlland AFB, NM 87117

4   Air Force Armament Laboratory
ATTN: J. Foster
       John Collins
       Joe Smith
       Guy Spitale
Eglin AFB, FL 32542

1   RADC (EMTLD, Lib)
Griffiss AFB, NY 13441

1   AUL (3T-AUL-60-118)
Maxwell AFB, AL 36112

1   AFML
ATTN: LLN, Dr. T. Nicholas
Wright-Patterson AFB, OH 45433

1   AFML
ATTN: LLN, Dr. John P. Henderson
Wright-Patterson AFB, OH 45433

1   Director
Environmental Science Service
   Administration
US Department of Commerce
Boulder, CO 80302

DISTRIBUTION LIST

Copies	Organization	Copies	Organization

6   Sandia National Laboratory
ATTN: Dr. L. Davison
       Dr. P.Chen
       Dr. L. Bertholf
       Dr. W. Herrmann
       Dr. J. Nunziato
       Dr. S. Passman
Albuquerque, NM   87115

1   Director
Jet Propulsion Laboratory
ATTN: Lib (TDS)
4800 Oak Grove Drive
Pasadena, CA 91109

1   Director
National Aeronautics and
   Space Administration
Lyndon B. Johnson Space Center
Houston, TX   77058

1   Aeronautical Research Associates
   of Princeton, Incorporated
ATTN: Ray Gogolewski
1800 Old Meadow Rd., #114
McLean, VA   22102

1   Honeywell, Inc.
Defense Systems Division
ATTN: Dr. Gordon Johnson
600 Second Street, NE
Hopkins, MN   55343

2   Orlando Technology, Inc.
ATTN: Dr. Daniel Matuska
       Dr. John J. Osborn
P.O. Box 855
Shalimar, FL   32579

7   SRI International
ATTN: Dr. George R. Abrahamson
       Dr. Donald R. Curran
       Dr. Donald A. Shockey
       Dr. Lynn Seaman
       Mr. D. Erlich
       Dr. A. Florence
       Dr. R. Caligiuri
333 Ravenswood Avenue
Menlo Park, CA   94025

1   System Planning Corporation
ATTN: Mr. T. Hafer
1500 Wilson Boulevard
Arlington, VA   22209

1   Terra-Tek, Inc.
ATTN: Dr. Arfon Jones
420 Wahara Way
University Research Park
Salt Lake City, UT   84108

3   California Institute of
   Technology
Division of Engineering and
   Applied Science
ATTN: Dr. J. Mikowitz
       Dr. E. Sternberg
       Dr. J. Knowles
Pasadena, CA   91102

1   University of Denver
Denver Research Institute
ATTN: Dr. R. Recht
P. O. Box 10127
Denver, CO   80210

3   Rensselaer Polytechnic Institute
ATTN: Prof. E. H. Lee
       Prof. E. Krempl
       Prof. J. Flaherty
Troy, NY   12181

1   Southwest Research Institute
ATTN: Dr. Charles Anderson
8500 Culebra Road
San Antonio, TX   78228

DISTRIBUTION LIST

Copies	Organization	Copies	Organization

2   Southwest Research Institute
Department of Mechanical
    Sciences
ATTN: Dr. U. Lindhholm
        Dr. W. Baker
8500 Culebra Road
San Antonio, TX   78228

1   University of Dayton
University of Dayton Rsch Inst
ATTN: Dr. S. J. Bless
Dayton, OH   45469

7   Brown University
Division of Engineering
ATTN: Prof. R. Clifton
        Prof. H. Kolsky
        Prof. L. B. Freund
        Prof. A. Needleman
        Prof. R. Asaro
        Prof. R. James
        Prof. J. Duffy
Providence, RI   02912

3   Carnegie Mellon University
Department of Mathematics
ATTN: Dr. D. Owen
        Dr. M. E. Gurtin
        Dr. B. D. Coleman
Pittsburgh, PA   15213

2   Catholic University of America
School of Engineering and
    Architecture
ATTN: Prof. A. Durelli
        Prof. J. McCoy
Washington, DC   20017

2   Forrestal Research Center
Aeronautical Engineering Lab.
Princeton University
ATTN: Dr. S. Lam
        Dr. A. Eringen
Princeton, NJ   08540

1   Harvard University
Division of Engineering and
    Applied Physics
ATTN: Prof. J. R. Rice
Cambridge, MA   02138

2   Iowa State University
Engineering Research Laboratory
ATTN: Dr. G. Nariboli
        Dr. A. Sedov
Ames, IA   50010

2   Lehigh University
Center for the Application
    of Mathematics
ATTN: Dr. E. Varley
        Dr. R. Rivlin
Bethlehem, PA   18015

1   New York University
Department of Mathematics
ATTN: Dr. J. Keller
University Heights
New York, NY   10053

1   North Carolina State University
Department of Civil Engineering
ATTN: Prof. Y. Horie
Raleigh, NC   27607

1   Pennsylvania State University
Engineering Mechanical Dept.
ATTN: Prof. N. Davids
University Park, PA   16802

2   Rice University
ATTN: Dr. R. Bowen
        Dr. C. C. Wang
P. O. Box 1892
Houston, TX   77001

DISTRIBUTION LIST

Copies	Organization	Copies	Organization

1   Southern Methodist University
Solid Mechanics Division
ATTN: Prof. H. Watson
Dallas, TX 75221

1   Temple University
College of Engineering
   Technology
ATTN: Dr. R. M. Haythornthwaite,
         Dean
Philadelphia, PA 19122

4   The Johns Hopkins University
ATTN: Prof. R. B. Pond, Sr.
       Prof. R. Green
       Prof. W. Sharpe
       Prof. J. Bell
34th and Charles Streets
Baltimore, MD 21218

1   Tulane University
Dept of Mechanical Engineering
ATTN: Dr. S. Cowin
New Orleans, LA 70112

3   University of California
ATTN: Dr. M. Carroll
       Dr. W. Goldsmith
       Dr. P. Naghdi
Berkley, CA 94704

1   University of California
Dept of Aerospace and
   Mechanical Engineering Science
ATTN: Dr. Y. C. Fung
P. O. Box 109
La Jolla, CA 92037

1   University of California
Department of Mechanics
ATTN: Dr. R. Stern
504 Hilgard Avenue
Los Angeles, CA 90024

1   University of California at
   Santa Barbara
Dept of Mechanical Engineering
ATTN: Prof. T. P. Mitchel
Santa Barbara, CA 93106

1   University of Delaware
Dept of Mechanical Engineering
ATTN: Prof. J. Vinson
Newark, DE 19711

1   University of Delaware
Dept of Mechanical and Aerospace
   Engineering
ATTN: Dr. Minoru Taya
Newark, DE 19711

2   University of Kentucky
Dept of Engineering Mechanics
ATTN: Dr. M. Beatty
       Prof. O. Dillon, Jr.
Lexington, KY 40506

2   University of Houston
Department of Mechanical
   Engineering
ATTN: Dr. T. Wheeler
       Dr. R. Nachlinger
Houston, TX 77004

1   University of Illinois
Dept. of Theoretical and
   Applied Mechanics
ATTN: Dr. D. Carlson
Urbana, IL 61801

1   University of Illinois
ATTN: Dean D. Drucker
Urbana, IL 61801

1   University of Illinois at
   Chicago Circle
College of Engineering
Dept. of Materials Engineering
ATTN: Dr. T. C. T. Ting
P. O. Box 4348
Chicago, IL 60680

2   University of Kentucky
Dept of Engineering Mechanics
ATTN: Dr. M. Beatty
       Prof. O. Dillon, Jr.
Lexington, KY 40506

DISTRIBUTION LIST

Copies	Organization	Copies	Organization

1   University of Maryland
Department of Mathematics
ATTN: Prof. S. Antman
College Park, MD 20740

1   University of Minnesota
Dept of Aerospace Engineering
  and Mechanics
ATTN: Prof. J. L. Erickson
107 Akerman Hall
Minneapolis, MN 55455

1   University of Pennsylvania
Towne School of Civil and
  Mechanical Engineering
ATTN: Prof. Z. Hashin
Philadelphia, PA 19105

4   University of Texas
Department of Engineering
  Mechanics
ATTN: Dr. M. Stern
       Dr. M. Bedford
       Prof. Ripperger
       Dr. J. T. Oden
Austin, TX 78712

1   University of Washington
Dept of Aeronautics and
  Astronautics
ATTN: Dr. Ian M. Fyfe
206 Guggenheim Hall
Seattle, WA 98105

2   Washington State University
Department of Physics
ATTN: Dr. R. Fowles
       Dr. G. Duvall
Pullman, WA 99163

2   Yale University
ATTN: Dr. B. T. Chu
       Dr. E. Onat
400 Temple Street
New Haven, CT 06520

Aberdeen Proving Ground

Dir, USAMSAA
  ATTN: DRXSY-D
         DRXSY-MP, H. Cohen
Cdr, USATECOM
  ATTN: DRSTE-TO-F
Cdr, CRDC, AMCCOM
  ATTN: DRSMC-CLB-PA
         DRSMC-CLN
         DRSMC-CLJ-L
Dir, MTD
  ATTN: STEAP-MT-G
         S. Walton

USER EVALUATION SHEET/CHANGE OF ADDRESS

This Laboratory undertakes a continuing effort to improve the quality of the reports it publishes. Your comments/answers to the items/questions below will aid us in our efforts.

1. BRL Report Number_____ Date of Report_____

2. Date Report Received_____

3. Does this report satisfy a need? (Comment on purpose, related project, or other area of interest for which the report will be used.)_____

_____

_____

4. How specifically, is the report being used? (Information source, design data, procedure, source of ideas, etc.)_____

_____

_____

5. Has the information in this report led to any quantitative savings as far as man-hours or dollars saved, operating costs avoided or efficiencies achieved, etc? If so, please elaborate._____

_____

_____

6. General Comments. What do you think should be changed to improve future reports? (Indicate changes to organization, technical content, format, etc.)

_____

_____

_____

CURRENT
ADDRESS

Name_____

Organization_____

Address_____

City, State, Zip_____

7. If indicating a Change of Address or Address Correction, please provide the New or Correct Address in Block 6 above and the Old or Incorrect address below.

OLD
ADDRESS

Name_____

Organization_____

Address_____

City, State, Zip_____

(Remove this sheet along the perforation, fold as indicated, staple or tape closed, and mail.)